



Prospective isolation of mouse and human hematopoietic stem cells using PLXDC2



Yosuke Tanaka ^{1,2,17}✉, Yasushi Kubota ^{3,4,17}✉, Riko Kikuchi⁵, Tomohiro Yabushita², Takaharu Kimura¹, Ivo Lieberam ⁶, Jillian L. Barlow⁷, Josh W. Bramley⁷, Tsuyoshi Fukushima¹, Chiaki Sakuma⁸, Takashi Shibata⁸, Masataka Nakagawa⁸, Yasunori Kurosawa^{8,9,18}, Toshiaki Maruyama ⁹, C. J. Okumura ⁹, Yuichiro Arima¹⁰, Yoshinori Sato¹¹, Yasuo Ono^{11,12}, Teruo Akuta ⁸, Hidenobu Mizuno ¹³, David G. Kent ⁷, Thomas M. Jessell^{14,19}, Susumu Goyama ¹⁵, Hidekazu Nishikii⁵, Shinya Kimura ³, Satoshi Yamazaki¹, Toshio Suda ² & Toshio Kitamura ¹⁶

Numerous strategies exist to isolate hematopoietic stem cells (HSCs) using complex combinations of markers and flow cytometry. However, robust identification of HSCs using imaging techniques is substantially more challenging which has prompted the recent development of HSC reporter mice. To date, very few molecules used in these reporters have been useful for human HSC identification. Here we report that PLXDC2 is a useful marker for both mouse and human cord blood HSCs. Using a green fluorescent protein (GFP) knock-in at the *Plxdc2* locus in mice (hereafter denoted as *Plxdc2*-GFP), we showed that *Plxdc2*-GFP is highly expressed in HSCs with 1 in 2.8 *Plxdc2*-GFP⁺CD150⁺ cells giving long-term multi-lineage reconstitution in transplantation. Moreover, we developed a novel human PLXDC2 antibody and showed that human PLXDC2⁺ HSCs have higher long-term multilineage reconstitution ability compared with PLXDC2⁻ HSCs in a xenograft model. This study identifies PLXDC2 as a highly relevant molecule in HSC identification.

A key aspect of stem cell biology is the definition of the different phenotypic and functional compartments, especially the most immature compartment, which replenishes all cells within a given tissue. In this regard, hematopoietic stem cells (HSCs) are the most comprehensively characterized tissue stem cells. Over the past three decades, the identification of HSCs has been improved by using both multicolor fluorescence-activated cell sorting analysis (FACS) and the *in vivo* bone marrow (BM) repopulation assay^{1–12}. c-Kit⁺, Sca-1⁺, lineage marker[–] (KSL) cells represented the first major step in HSC identification, but have been further enriched by additional negative (CD34², Flk2¹³, CD48, and CD41⁴) and positive (CD150⁴, CD105¹⁴, CD201¹⁵, and Esam1^{16,17}) markers. Most of the FACS-based HSC purification methods use the CD150⁺CD34^{low/–}c-Kit⁺Sca-1⁺lineage marker-negative (Lin[–]) BM population to purify adult mouse HSCs, which contain cells with long-term multilineage reconstitution and self-renewal ability^{4,18,19}. However, the CD150⁺CD34^{low/–}c-Kit⁺Sca-1⁺Lin[–] BM cells still contain cells that are not long-term HSCs (LT-HSCs). Additionally, identification of negatively stained cells is straightforward with FACS analysis, but is substantially more complicated with non-quantitative immunofluorescence on fixed and embedded tissue sections, despite the urgent need to understand HSC behavior in the context of the *in vivo* HSC-microenvironment (niche). Several HSC-specific reporters, such as *Fgd5*-

mCherry or ZsGreen, *Hoxb5*-mCherry, and α-catulin-GFP, already exist as powerful tools for visualizing HSCs throughout the BM^{20–22}. However, these HSC visualization technologies are not accessible to all researchers because they require mice. Therefore, simple methods using a few antibodies for positive markers are preferable to meet the above requirements.

Human transplantation and xenograft repopulation assays show that human HSCs are CD34⁺, but the majority of CD34⁺ cells are lineage-restricted progenitors, and HSCs consist of a minor component of the population. The standard purification strategy to date for human HSCs uses the cell surface marker profile Lin[–]CD34⁺CD38[–]CD90⁺CD45RA^{6–8,11,23} and the most recent purification method for human HSCs uses CD49f in addition to these markers to arrive at a population that is ~10% functional HSCs when human cord blood (CB) is used as the starting material¹¹. While this is a major milestone, the enriched CD34⁺CD38[–]CD90⁺CD45RA[–]CD49f⁺ population remains more heterogeneous than mouse HSCs, therefore requiring new markers to further purify functional human HSCs.

Our previous screening on HSC-specific genes identified several cell surface genes²⁴. We noted plexin domain containing 2 (*Plxdc2*) among them. PLXDC2 is a single-pass type I membrane protein that encodes a 350-amino acid-long plasma membrane protein. PLXDC2 plays an important

role in cell proliferation and differentiation during nervous system development^{25,26}. PLXDC2 is also known as one of the membrane receptors of pigment epithelial-derived factor, an endogenous anti-angiogenesis factor²⁷. Moreover, PLXDC2 is an activating ligand for ADGRD1 displayed on cumulus cells²⁸. In addition, PLXDC2 has a regulatory function and a significant impact on the modulation of the host immune response against *Helicobacter pylori*²⁹. However, the function of PLXDC2 in the hematopoietic system remains unknown.

In the present study, we identified PLXDC2 as an HSC purification marker using a *Plxdc2*-GFP knock-in mouse line²⁶ and found that the combination of two positive markers, *Plxdc2*-GFP and CD150, provided sufficient purification of functional HSCs without any additional markers. Moreover, PLXDC2 was also highly expressed in human HSCs derived from both CB and BM. We showed that the anti-PLXDC2 antibody, clone 4G3, which we previously developed³⁰, was useful for further purification of human functional HSCs from the conventional human HSC fraction.

Results

Plxdc2 is highly expressed in mouse HSCs

Our previous gene expression analysis between CD34⁻ KSL cells as HSCs and other hematopoietic cells identified HSC-specific genes²⁴. In the present study, we studied *Plxdc2* as a candidate surface marker for purification of HSCs among them. *Plxdc2* is a single-pass type I membrane protein that is expressed in tumor vessels but not in most normal tissues. Quantitative reverse transcription PCR revealed that *Plxdc2* was highly expressed in CD34⁻ KSL cells and CD4⁺CD8⁺ double positive T cells in mouse hematopoietic cells (Fig. 1A). We further confirmed that *Plxdc2* was highly expressed in LT-HSCs compared with short-term HSCs (ST-HSCs), multipotent progenitors (MPPs) and progenitors (Fig. 1B). Moreover, public gene expression data showed that *Plxdc2* was highly expressed in HSCs and niche cells, including CAR (CXCL12-abundant reticular) cells, fibroblasts, and Schwann cells in mouse BM (Supplementary Fig. 1A-C).

To assess *Plxdc2* expression in hematopoiesis in detail, we analyzed *Plxdc2*-GFP knock-in mice. Both *Plxdc2*^{GFP/+} and *Plxdc2*^{GFP/GFP} mice were born and survived into adulthood with expected Mendelian frequencies. *Plxdc2*^{GFP/+} and *Plxdc2*^{GFP/GFP} mice showed normal hematopoiesis (Supplementary Tables 1 and 2). Colony-forming assay of whole BM cells revealed no significant difference between *Plxdc2*^{+/+} and *Plxdc2*^{GFP/GFP} littermates in the frequency of lineage-restricted hematopoietic progenitors (Supplementary Fig. 2A). *Plxdc2*^{GFP/+} and *Plxdc2*^{GFP/GFP} mice showed normal HSC frequency and normal HSC function upon transplantation into lethally irradiated mice, indicating that *Plxdc2* is dispensable for HSC function (Supplementary Fig. 2B, C).

Mature hematopoietic cells in the BM from *Plxdc2*^{GFP/+} mice did not express *Plxdc2*-driven GFP (hereafter referred to as “*Plxdc2*-GFP”), whereas most of the T cells, except CD4⁻CD8⁻c-Kit⁻CD25⁻ cells in the thymus, expressed *Plxdc2*-GFP (Supplementary Fig. 3A, B). Overall, just 0.19% of total BM cells in *Plxdc2*^{GFP/+} mice were *Plxdc2*-GFP⁺ (Fig. 1C). Neither common lymphoid progenitors (CLPs) nor myeloid progenitors (MPs) expressed *Plxdc2*-GFP (Supplementary Fig. 3C). *Plxdc2*-GFP expression was highly enriched in KSL cells (9.23%), CD150⁺ KSL cells (43%) and CD34⁻CD150⁺ KSL cells (72.7%) suggesting that it was highly enriched in LT-HSCs (Fig. 1D). Of note, *Plxdc2*-GFP expression in KSL cells was negatively correlated with CD34 expression and most of the *Plxdc2*-GFP cells were CD150⁺ (Fig. 1E), further supporting the notion that *Plxdc2*-GFP⁺ cells are highly enriched in HSCs.

Functional HSC activity is highly restricted to *Plxdc2*-GFP⁺CD150⁺ cells

To examine HSC potential of *Plxdc2*-GFP⁺ cells in the BM, 500 *Plxdc2*-GFP⁺ cells or 2×10^5 *Plxdc2*-GFP⁻ cells were transplanted into lethally irradiated mice alongside 2×10^5 cells of competitor cells (Fig. 2A). Long-term multilineage chimerism was observed in peripheral blood (PB) from *Plxdc2*-GFP⁺ cell-transplanted mice over 21 weeks, whereas only short-term lymphoid lineage chimerism was observed at low levels in PB from

Plxdc2-GFP⁻ cell-transplanted mice (Fig. 2B). Limiting dilution analysis revealed that 1 in 3.53 *Plxdc2*-GFP⁺ KSL cells gave long-term multilineage reconstitution of irradiated primary recipients (Supplementary Table 3) and single-cell transplants showed that 1 in 2.05 *Plxdc2*-GFP⁺CD150⁺ KSL cells gave long-term multilineage reconstitution of irradiated primary recipients. To simplify the purification method of HSCs to a two-color strategy, we assessed the combination of *Plxdc2*-GFP and CD150. Nearly all of the *Plxdc2*-GFP⁺CD150⁺ cells were also CD34⁻CD150⁺ KSL cells, and *Plxdc2*-GFP⁺CD150⁻ cells were c-Kit⁻ cells (Fig. 2C). Limiting dilution analysis of the *Plxdc2*-GFP⁺CD150⁺ fraction of whole BM cells revealed that the HSC frequency of *Plxdc2*-GFP⁺CD150⁺ cells was 1 in 2.8 (Supplementary Table 3). Single-cell transplantation studies revealed that 44.7% (17/38) of *Plxdc2*-GFP⁺CD150⁺ cells and 48.8% (21/43) of *Plxdc2*-GFP⁺CD150⁺ KSL were functional HSCs capable of long-term multilineage reconstitution (Supplementary Table 3), indicating that the *Plxdc2*-GFP⁺CD150⁺ fraction was roughly equivalent to the *Plxdc2*-GFP⁺CD150⁺ KSL fraction. Collectively, these data suggest that *Plxdc2*-GFP⁺CD150⁺ cells in the whole BM are functional HSCs and therefore the combination of *Plxdc2*-GFP and CD150 is sufficient to purify functional HSCs in the whole BM.

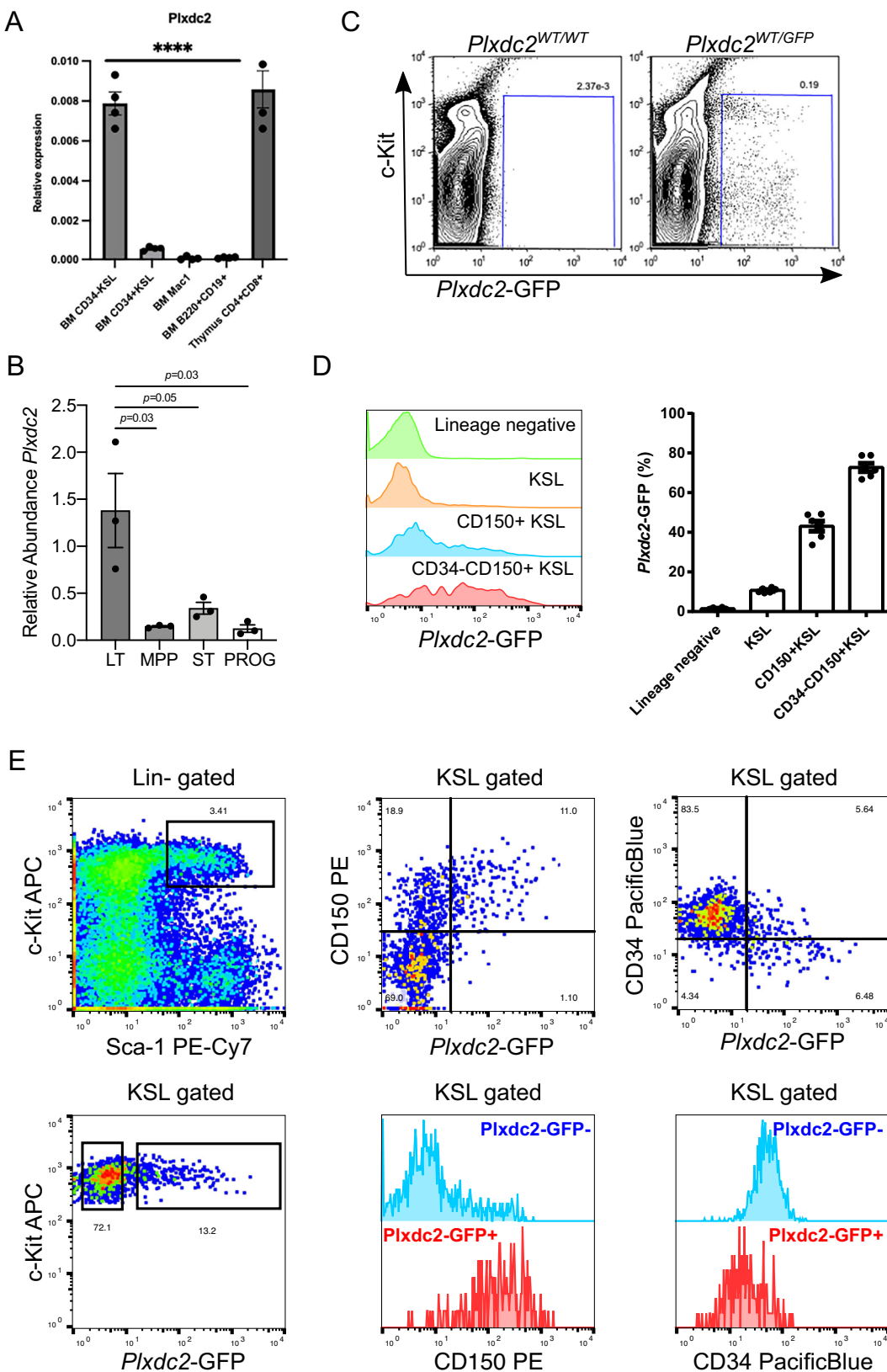
To further validate the *Plxdc2*-GFP and CD150 combination for HSC identification, we compared this strategy with the widely used SLAM-based method described by Kiel et al.⁴. We analyzed the spatial distribution of *Plxdc2*-GFP⁺CD150⁺ cells relative to CD150⁻CD48⁻CD41⁻Lin⁻ HSCs in BM sections. *Plxdc2*-GFP⁺CD150⁺ cells were overlapping with CD150⁻CD48⁻CD41⁻Lin⁻ cells (Fig. 2D), consistent with their enrichment in HSCs observed by flow cytometry. In addition, *Plxdc2*-GFP⁺CD150⁺ cells expressed other HSC-associated markers, including CD31 and Emcn (Supplementary Fig. 3D, Supplementary Movie 1). These findings indicate that *Plxdc2*-GFP combined with CD150 can reliably identify HSCs in both dissociated and tissue-based analyses.

Plxdc2 stably marks mobilized HSCs

To further extend analysis for the clinical setting, we examined whether *Plxdc2*-GFP also marked mobilized HSCs in the spleen after cyclophosphamide/granulocyte-colony stimulating factor (G-CSF) treatment. To this end, we administered a single dose of cyclophosphamide on day 0 and constitutive administration of G-CSF for 1 week from day 1 and then analyzed *Plxdc2*-GFP expression in mobilized HSCs in the spleen (Fig. 3A). No *Plxdc2*-GFP⁺ cells were detected in the spleen in the steady-state condition, whereas 0.11% of cells were *Plxdc2*-GFP⁺ after administration of G-CSF (Fig. 3B). 8.15% of mobilized KSL cells in the spleen expressed *Plxdc2*-GFP and CD150. 500 *Plxdc2*-GFP⁺ cells isolated from mobilized spleen gave long-term multilineage chimerism in lethally irradiated mice, whereas 2×10^5 cells of *Plxdc2*-GFP⁻ cells in mobilized spleen contained no HSCs (Fig. 3C, D). These data indicate that *Plxdc2*-GFP expression consistently marks HSCs under the mobilization condition.

PLXDC2 is heterogeneously expressed on human HSCs

In order to determine whether PLXDC2 is relevant for human HSCs, we extended our analysis by first assessing its expression using a newly established rabbit monoclonal antibody for human PLXDC2 (clone 4G3)³⁰. Although this antibody was originally validated in HEK293 cells over-expressing PLXDC2, we further evaluated its specificity by Western blot using human peripheral blood mononuclear cells (PBMCs) and human platelets. Multiple bands ranging from 75 to 100 kDa were detected, depending on cell type, consistent with the predicted molecular weight of glycosylated PLXDC2 (Supplementary Fig. 4A-D). This heterogeneity likely reflects glycosylation status and protein conformation. Notably, clone 4G3 was identified by flow cytometric screening and shows strong binding to native PLXDC2 on the cell surface, suggesting preferential recognition of conformational epitopes. Moreover, the specificity was confirmed by flow cytometry using PLXDC2-overexpressing SKM-1 cells, showing dose-dependent signal reduction upon antibody dilution (Supplementary Fig. 4E). These data support the antibody's suitability for native-state



applications such as flow cytometry-based HSC purification. PLXDC2 expression was highest on the conventional human HSCs (CD34⁺CD38⁻CD90⁺CD45RA⁻CD49f⁺ cells) among hematopoietic stem and progenitor cells (HSPCs) in the CB (Fig. 4A, Supplementary Fig. 5A). Interestingly, this expression pattern varied in the BM and G-CSF-

mobilized PB HSPCs. MEPs (Megakaryocyte-erythroid progenitor cells) showed the highest expression of PLXDC2 in the BM HSPCs, whereas GMPS (Granulocyte-monocyte progenitor cells) did in the G-CSF-mobilized PB HSPCs (Supplementary Fig. 5B). Unlike in mouse, *PLXDC2* expression was not entirely restricted to the HSC compartment,

Fig. 1 | Plxdc2 is enriched for functional HSCs. Quantitative PCR analysis showing the abundance of *Plxdc2* relative to *Hprt* in the indicated populations in BM and thymus (A) and in populations of BM stem and progenitor cells (B). LT: LT-HSCs (Lin⁻c-Kit⁺Sca1⁺CD135⁻CD34⁻), MPP multipotent progenitor cells (Lin⁻c-Kit⁺Sca1⁺CD135⁻CD34⁺), ST: ST-HSCs (Lin⁻c-Kit⁺Sca1⁺CD135⁻CD34⁺), and PROG progenitors (CMP, GMP, and MEP, Lin⁻c-Kit⁺Sca1⁻). Source data are provided as a Supplementary Data file. C Representative FACS plots of *Plxdc2*-GFP⁺ cells in the BM. Left: *Plxdc2*^{+/+} mice, right: *Plxdc2*^{+/}/GFP mice. D The percentage of *Plxdc2*-GFP⁺ cells in the indicated cell types. Left: representative

FACS plots, right: a bar plot ($n = 6$ each). Source data are provided as a Supplementary Data file. E Representative FACS plots for expression of HSC markers on *Plxdc2*-GFP⁺ cells. Expression profiles of KSL cells for *Plxdc2*-GFP, CD34, and CD150 (upper panels). Expression profiles of KSL cells for *Plxdc2*⁺ KSL cells (blue) and *Plxdc2*⁻ KSL cells (red) for CD34 and CD150 (lower panels). Data are shown as the mean \pm SEM. *P* values were calculated using one-way ANOVA with Tukey's correction for multiple comparisons. **P* < 0.05, ***P* < 0.01, ****P* < 0.001, *****P* < 0.0001.

showing some expression in progenitor cells and CD14⁺ monocytes (Supplementary Fig. 5B–D). Flow cytometric analysis of the PBMCs showed that PLXDC2 was detected on CD41⁺ cells (12.6%), CD56⁺ cells (2.8%), CD19⁺ cells (13.9%), CD3⁺ cells (3.05%), CD33⁺CD66b⁻ cells (15.5%) and CD14⁺CD15⁺ cells (49.4%) (Supplementary Fig. 5E). In order to test whether PLXDC2 expression tracked with HSC function, we separated human HSCs derived from CB into PLXDC2^{+/high} (referred to here as PLXDC2⁺) and PLXDC2^{-low} (referred to here as PLXDC2⁻) and performed functional assays (Fig. 4B). We first evaluated their hematopoietic colony-forming capacity in serial replating assays. PLXDC2⁻ cells formed 1.6-fold more colonies than PLXDC2⁺ cells in the first round. In contrast, PLXDC2⁺ cells formed 1.6-fold more colonies than PLXDC2⁻ cells in the second round of plating (Fig. 4C), suggesting that PLXDC2⁺ cells were more immature than PLXDC2⁻ cells. We next evaluated their capacity for long-term multilineage reconstitution by transplanting them into NOD-scid-IL2R γ C^{-/-} (NSG) recipients (200 cells of either PLXDC2⁺ HSCs or PLXDC2⁻ HSCs per mouse). PLXDC2⁺ cells gave higher human CD45⁺ chimerism in PB than PLXDC2⁻ cells during the observation period (Fig. 4D). Although levels of chimerism remained high in the PB of mice transplanted with PLXDC2⁺ HSCs, engraftment of PLXDC2⁻ HSCs peaked at 2 months and then declined. The chimerism pattern of PLXDC2⁻ HSCs indicated that PLXDC2⁻ HSCs were mainly ST-HSCs. Moreover, PLXDC2⁺ cells gave much higher mean chimerism in hematopoietic organs than PLXDC2⁻ cells (Fig. 4E). PLXDC2⁺ cells gave more B cell output (Chimerism of CD19⁺ cells) than PLXDC2⁻ cells (Fig. 4F), whereas erythrocyte output was similar between PLXDC2⁺ and PLXDC2⁻ cells (Fig. 4G). Limiting dilution assays demonstrated that 1 in 49.9 PLXDC2⁺ cells could give rise to long-term multilineage engraftment compared with 1 in 249.1 PLXDC2⁻ cells ($P = 0.00348$, Fig. 4H). Our HSC frequency (2%) was much less than that shown by the Dick group (10%)¹¹. This discrepancy may be due to differences in experimental conditions, such as an irradiation dose and an injection method.

Next, we evaluated the surface expression of PLXDC2 on HSPCs during HSC culture using flow cytometric analysis to determine whether PLXDC2 is a useful marker in this context. PLXDC2 expression showed a positive correlation with CD90 and CD201 after 6 days in culture (Supplementary Fig. 6A). Furthermore, we compared the expression of CD112, a recently reported marker of HSC latency, between PLXDC2⁺ and PLXDC2⁻ HSCs. Both populations expressed CD112 at similar levels (Supplementary Fig. 7A, B). Taken together, although PLXDC2 is not a specific marker for human HSCs, it serves as a useful marker for further purification of human HSCs and may be beneficial in the context of HSC culture.

PLXDC2⁺ HSCs express more HSC signature genes than PLXDC2⁻ HSCs

To examine the expression pattern of PLXDC2 mRNA in human HSPCs, we analyzed publicly available single-cell RNA-seq data from fresh CB CD34⁺ cells. PLXDC2 was highly expressed in Cluster 1, which was defined as HSPCs based on high expression of *MECOM*, *MLLT3*, and *HLF*, indicating that PLXDC2 is enriched in human HSPCs (Fig. 5A, B). To examine transcriptomic differences between PLXDC2⁺ and PLXDC2⁻ HSCs derived from the CB, we performed RNA-Seq analysis. Although transcriptomes of PLXDC2⁺ HSCs and PLXDC2⁻ HSCs were highly similar, THBS1, SORBS2, SGSH, and SAMHD1 were identified as highly differentially expressed genes (DEGs) in PLXDC2⁺ HSCs (FDR < 0.01), whereas CPA3,

ABCA1, CDK6, and IRF8 were highly DEGs in PLXDC2⁻ HSCs (FDR < 0.01) (Fig. 5C, D). Interestingly, CDK6 expression has been shown to mark active HSCs in mouse and human studies^{31–33} and IRF8 is a differential marker for myeloid cells^{34,35}. The gene expression data therefore suggest that PLXDC2⁻ HSCs express a more differentiated gene signature than PLXDC2⁺ HSCs. Interestingly, although the functions of THBS1, SORBS2, SGSH, and SAMHD1 in HSCs were not well understood, their functions were related to important HSC signatures such as active TGF β signaling, adhesion character, activation of lysosomal function, and resistance to viral infection (Supplementary Table 4). Next, we investigated the biological pathways differentially represented between PLXDC2⁺ HSCs and PLXDC2⁻ HSCs using gene set enrichment analysis (GSEA) (Fig. 5E, FDR < 0.1). Again, PLXDC2⁺ HSCs showed an enrichment for the HSC signature. Conversely, we found downregulation of essential biosynthetic processes such as mRNA processing, oxidative phosphorylation, and MYC targets in PLXDC2⁺ HSCs compared with PLXDC2⁻ HSCs. Together, these data reinforced the functional data above, indicating that the PLXDC2⁺ fraction contains more cells expressing HSC-related genes than the PLXDC2⁻ fraction.

Discussion

Our study shows that PLXDC2 is a useful marker for identifying both mouse and human HSCs. Because of the limited availability of human HSCs in the BM or fetal liver and their different purification methods from those of mouse HSCs, the features of human HSCs are not well understood. In order to make robust comparisons across species, it is therefore essential to identify common markers. To date, however, only a few common markers, such as EPCR and ESAM, have been reported^{15,16,36–39}. Interestingly, these markers, including PLXDC2, are all endothelial markers, suggesting that HSCs retain some aspects of an endothelial program, which is perhaps reflective of their origin from endothelial cells during development and may be a useful feature that allows their discrimination from other hematopoietic cells. Therefore, developing common purification methods between mouse and human HSCs using these endothelial markers is useful for deepening our understanding of human HSCs.

Plxdc2 in combination with CD150 is enough to highly purify mouse functional HSCs compared with the conventional multi-antibody combination. 1 in 2.8 *Plxdc2*-GFP⁺CD150⁺ cells in whole BM were functional HSCs (Supplementary Table 3). This HSC frequency is equivalent to the frequency reported using α -catulin in combination with c-Kit (1 in 3.1 cells)²² and collectively represent the best two-color strategies to date. *Plxdc2* is a more attractive marker for purification of HSCs than α -catulin, because *Plxdc2* is a membrane protein, whereas α -catulin is an intracellular protein. In this study, we developed a flow cytometry approach using a recently available anti-human PLXDC2 antibody. Developing a flow cytometric analysis available antibody against mouse *Plxdc2* will allow us to highly purify mouse functional HSCs in combination with CD150 and to easily detect mouse functional HSCs without the need for a reporter mouse. Our two-color strategy is also useful for imaging studies. It is hoped that the new antibody will improve the sensitivity and enable HSC detection.

Our study also shows that PLXDC2 further purifies human HSCs from the conventional human CD34⁺CD38⁻CD90⁺CD45RA⁻CD49f⁺ fraction, which may be one of the most purified fractions for human functional HSCs. The finding that further enrichment of functional human HSCs could be achieved by using an anti-PLXDC2 antibody will aid researchers looking to

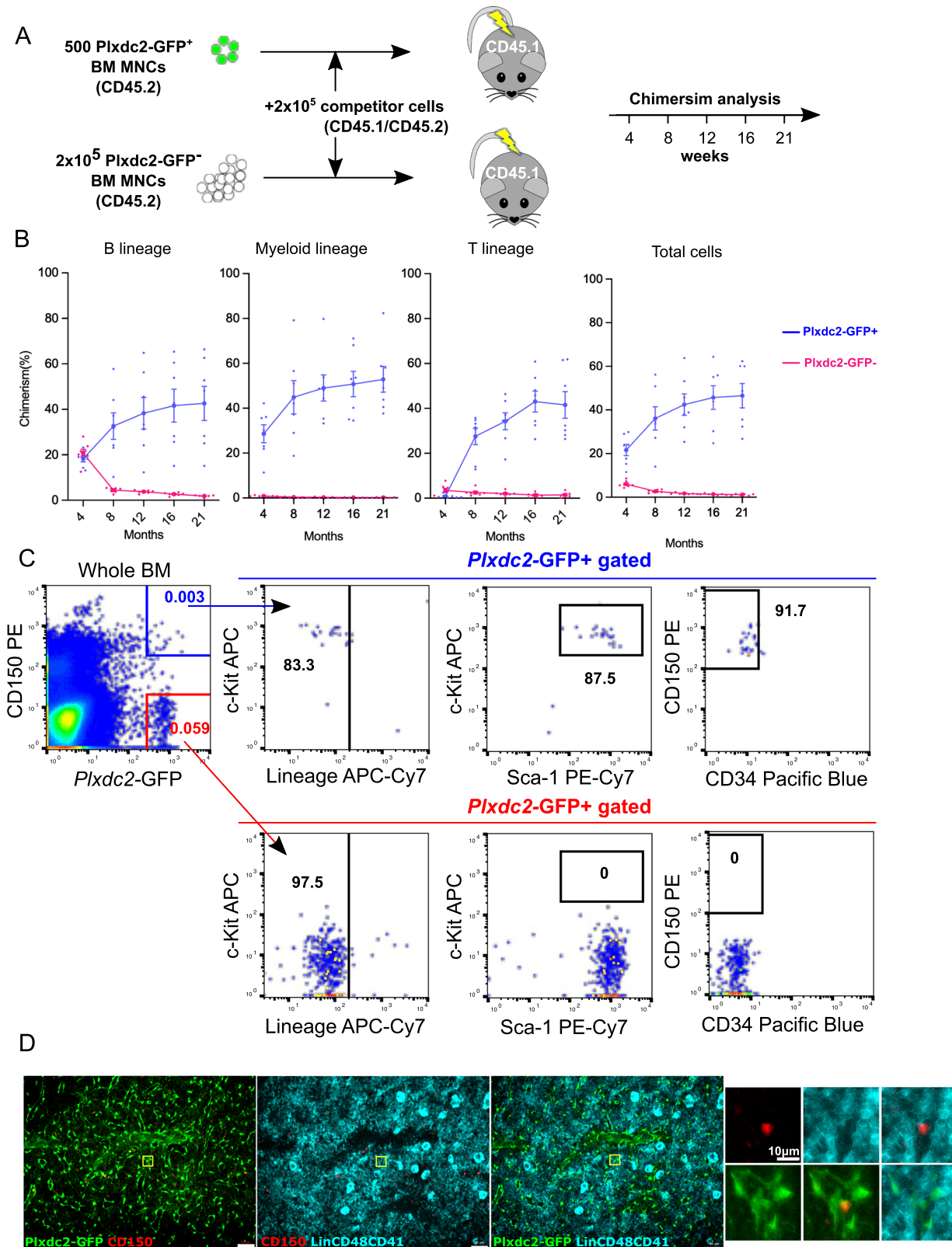


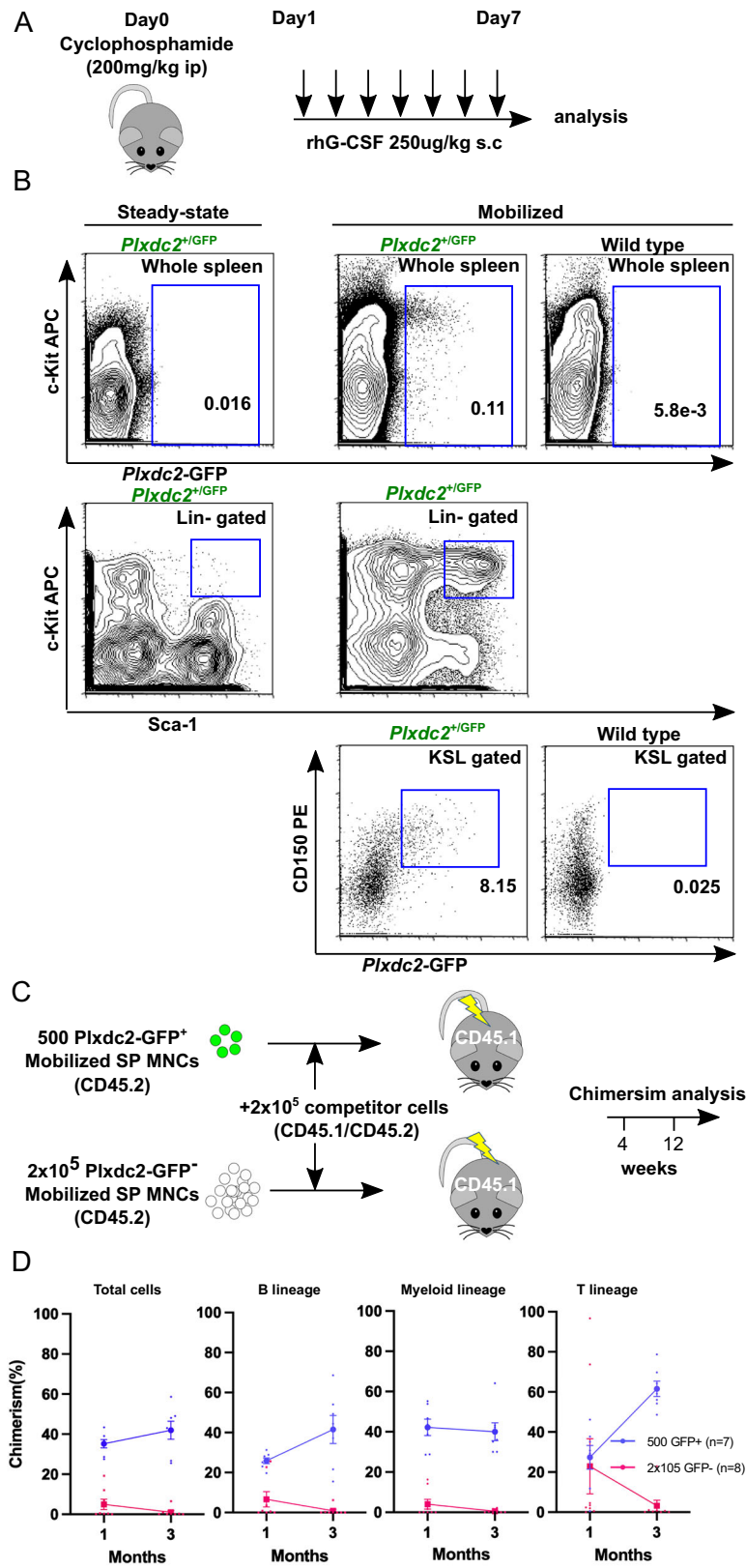
Fig. 2 | *Plxdc2*-GFP⁺ cells are highly enriched for functional HSCs.

A Experimental design. **B** Chimerism kinetics of donor cells in the indicated lineages. Source data are provided as a Supplementary Data file. **C** Expression profiles of Lin, c-Kit, Sca-1, CD34, and CD150 on *Plxdc2*-GFP⁺ whole BM cells and *Plxdc2*-GFP⁻ whole BM cells. **D** Representative imaging of femoral BM slice from *Plxdc2*^{+/+}/GFP mice stained with CD150, lineage markers, CD48, and CD41. *Plxdc2*-GFP⁺ cells (green) and CD150⁺ cells (red) are shown, revealing substantial spatial

overlap. CD150⁺ cells (red) are co-stained with lineage markers (Lin, cyan), CD48 (cyan), and CD41 (cyan), enabling identification of SLAM-defined HSCs (CD150⁺Lin⁻CD48⁻CD41⁻). High-magnification insets of the yellow boxed region demonstrate a cell that is simultaneously *Plxdc2*-GFP⁺ (green), CD150⁺ (red), and negative for lineage, CD48, and CD41 (cyan), confirming that *Plxdc2*-GFP⁺CD150⁺ cells overlap with SLAM-defined HSCs. Scale bars = 50 μm and 10 μm (magnified images). Data are shown as the mean ± SEM.

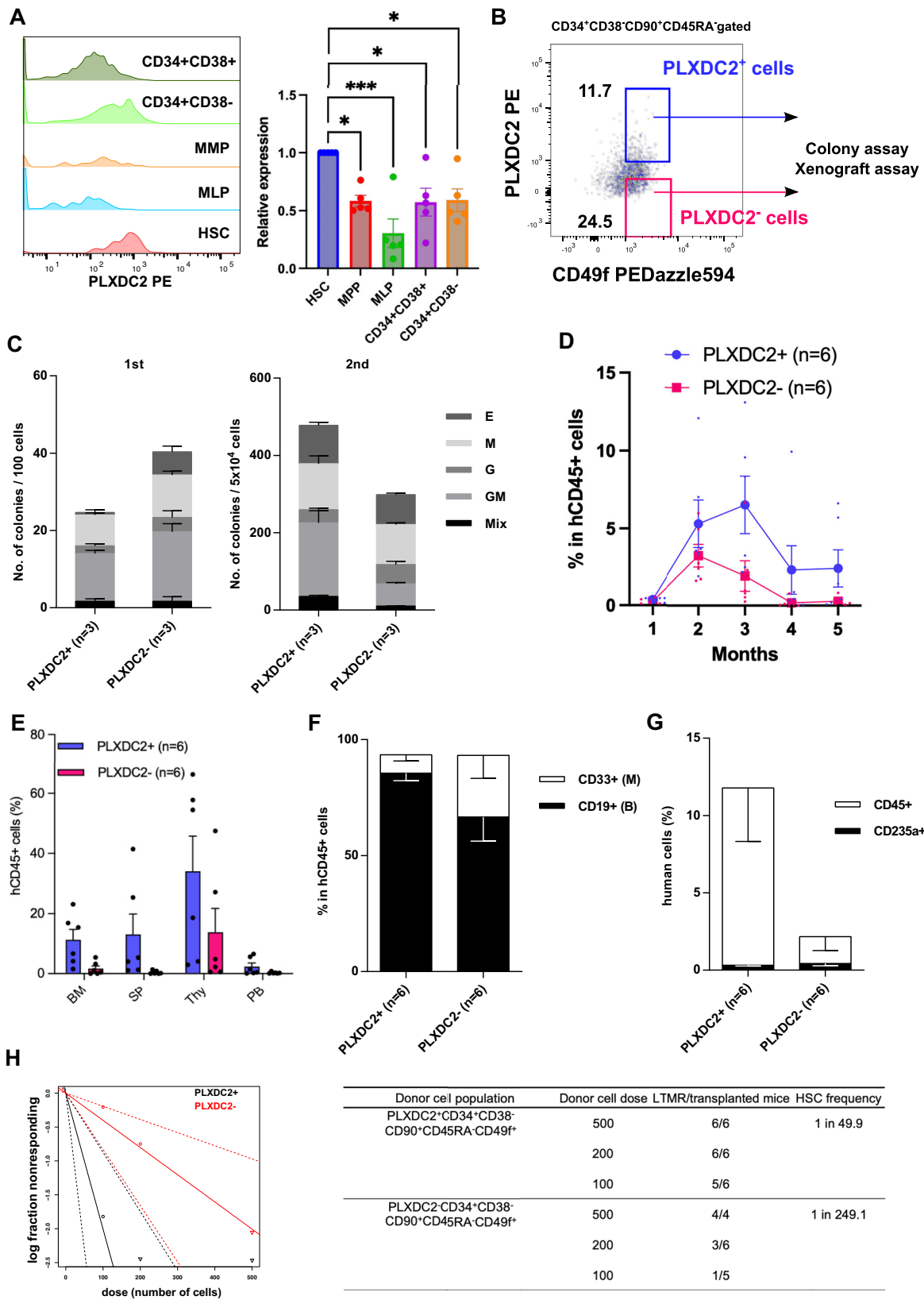
Fig. 3 | *Plxdc2*-GFP marks mobilized HSCs.

A Experimental design of G-CSF administration. B Representative FACS plots for *Plxdc2*-GFP⁺ cells in steady-state and mobilized spleens from *Plxdc2*^{+/GFP} mice. C Experimental design of transplantation of mobilized spleen cells. D Chimerism kinetics of donor cells in the indicated lineages from the transplants in (C). Source data are provided as a Supplementary Data file. Data are shown as the mean \pm SEM.



further purify functional human HSCs for cellular and molecular studies. Moreover, PLXDC2⁺ HSCs showed a negative correlation with gene signatures for mRNA processing, upregulation of Myc-regulated genes, and oxidative phosphorylation, indicating that PLXDC2⁺ HSCs are likely to be quiescent (Fig. 5E). The mature cell output ratio between B cells and myeloid

cells in PLXDC2⁺ HSCs was B lymphoid dominant, consistent with that of conventional CD34⁺CD38⁻CD90⁺CD45RA⁻CD49f⁺ HSCs. In contrast, repopulation in PLXDC2⁻ HSCs was balanced, which could be explained by higher expression of IRF8 in PLXDC2⁻ HSCs compared to PLXDC2⁺ HSCs.



The timing of quiescence exit in human HSC subsets is regulated by CDK6 levels³¹. As PLXDC2⁺ HSCs show lower CDK6 expression than PLXDC2⁻ HSCs, they are likely more quiescent. Four genes, THBS1, SORBS2, SGSH, and SAMHD1, are highly upregulated in PLXDC2⁺ HSCs. THBS1 activates latent TGF β ⁴⁰, which is essential

for HSC maintenance⁴¹. SORBS2, an adapter protein involved in focal adhesion⁴², suppresses cancer metastasis⁴³ and may support HSC anchoring in the niche^{44,45}. SGSH, which degrades heparan sulfate in lysosomes, is critical for lysosomal function; active lysosomes help maintain HSC stemness after division⁴⁶. SAMHD1, a restriction

Fig. 4 | Enrichment of human functional HSCs by PLXDC2 expression.

A PLXDC2 expression on the indicated cell types was detected by anti-PLXDC2 antibody in human cord blood mononuclear cells. Left: representative FACS plots. Right: quantitative data from five different cord blood samples. Source data are provided as a Supplementary Data file. **B** Representative FACS plots for gating PLXDC2⁺ HSCs and PLXDC2⁻ HSCs. **C** Hematopoietic colony-forming assays using PLXDC2⁺ HSCs and PLXDC2⁻ HSCs. 1st colony assays (left: 100 cells/dish) and 2nd colony assays (right: 50,000 cells/dish). Source data are provided as a Supplementary Data file. **D** Kinetic analysis of peripheral blood engraftment (measured as percent of CD45⁺ cells) by PLXDC2⁺ HSCs and PLXDC2⁻ HSCs after transplantation into NSG mice (200 cells per recipient, $n = 6$ each). Source data are

provided as a Supplementary Data file. **E** Engraftment of PLXDC2⁺ HSCs and PLXDC2⁻ HSCs assessed in NSG mice 20 weeks after transplant. BM, BM; SP, spleen; PB peripheral blood. Source data are provided as a Supplementary Data file. **F** Lineage potential of PLXDC2⁺ HSCs and PLXDC2⁻ HSCs assessed in NSG mice 20 weeks after transplant. B cells (B: black bars) and myeloid cells (M: white bars). Source data are provided as a Supplementary Data file. **G** The human graft consisted of CD235a⁺ erythroid (black bars) and CD45⁺ myelo-lymphoid cells (white bars). Source data are provided as a Supplementary Data file. **H** Long-term repopulating cell frequency in PLXDC2⁺ HSCs and PLXDC2⁻ HSCs measured by LDA. Data are shown as the mean \pm SEM.

factor for HIV^{47,48}, and an interferon-stimulated gene, is selectively expressed in HSCs⁴⁹. Thus, these genes may cooperatively support the stem cell state of PLXDC2⁺ HSCs.

Taken together, our data show that *Plxdc2* is a potent marker for enrichment of both mouse and human HSCs. Until we have common markers across species, we will be limited in our ability to make comparisons between mouse and human HSCs. Therefore, the finding of PLXDC2 as a common marker between mouse and human has a great impact in this regard.

Methods

Animals

All animal studies were approved by the Animal Care Committee of the Institute of Medical Science at the University of Tokyo and were conducted in accordance with the Regulation on Animal Experimentation at the University of Tokyo based on International Guiding Principles for Biomedical Research Involving Animals. C57BL/6J mice were purchased from SLC Inc., Japan. NOD.Cg-PrkdcscidIl2rgtm1Wjl (NSG) mice were purchased from The Jackson Laboratory Inc., Japan. *Plxdc2*-GFP mice were kindly provided by Thomas M Jessell (Columbia University). All mice were obtained at the age of 8–10 weeks and maintained in a specific-pathogen-free environment with free access to food and water. Housing conditions were temperature 22 \pm 2 °C, humidity 55 \pm 5%, light/dark cycle 12 h/12 h (8 a.m.–20 p.m. light). All mice were euthanized under isoflurane anesthesia followed by cervical dislocation, in accordance with institutional animal care and use guidelines.

Cell lines

PlatE cells were maintained in Dulbecco's Modified Eagle's Medium supplemented with 10% fetal bovine serum (FBS) and 1% penicillin–streptomycin(P/S). SKM-1 (JCRB0118, JCRBCell Bank) cells were maintained in RPMI-1640 medium supplemented with 10% FBS and 1% P/S.

Preparation of retrovirus

The cDNA encoding human PLXDC2 was cloned into the EcoRI site of the MSCV-IRES-GFP vector. Retroviral packaging cells (Plat-E) were transiently transfected with either empty or MSCV-PLXDC2-IRES-GFP plasmids using polyethylenimine (Sigma-Aldrich).

Quantitative PCR

Plxdc2 expression levels in LT-HSCs and MPPCs were quantified relative to expression of the hypoxanthine–guanine phosphoribosyltransferase (Hprt) housekeeping gene via qPCR. The primer pairs were as follows: *Plxdc2*-Forward CCC GGA AGA GGT ACA GTC AAA, *Plxdc2*-Reverse GAA TTG CAT GGT GGT CGT GT, Hprt-Forward GTT GGA TAC AGG CCA GAC TTT GTT G, Hprt-Reverse GAG GGT AGG CTG GCC TAT AGG CT. qPCRs were performed using 10 μ l of 2x SYBR Green master mix, 1 μ l of LT-HSC or MPPC cDNA, 1 μ l each of *Plxdc2* or Hprt forward and reverse primers concentrated at 1000 nM, and 7 μ l of nuclease-free water per well. Negative control wells containing 1 μ l of nuclease-free water instead of cDNA were constructed to rule out contamination of our reagents. Progenitor cDNA samples were sourced

from four biologically distinct mice, and LT-HSC cDNA samples were sourced from three biologically distinct mice in an attempt to enable a valid statistical analysis of our qPCRs. The progenitor and LT-HSC cDNA libraries used in these qPCRs were also derived courtesy of Dr Jillian Barlow. qPCRs using progenitor cDNA were performed in triplicate, whilst qPCRs using LT-HSC cDNA were performed in duplicate to identify anomalous results. qPCRs were run using the StepOnePlus™ Real-Time PCR System (Applied Biosystems™) on a fast ramp speed for 45 cycles before quantifying *Plxdc2* expression relative to Hprt expression (mean $\Delta\Delta Ct$) in Microsoft Excel. The statistical significance of differential *Plxdc2* expression between LT-HSCs and MPPCs was determined in R-studio using the Mann–Whitney *U* test.

Hematopoietic progenitor assays

Colony-forming activity (CFU-C) assays were performed using MethoCult M3434 (Stem Cell Technologies). A total of 2×10^4 BM mononuclear cells (MNCs) were plated on 35-mm culture dishes and then incubated at 37 °C in humidified chambers containing 5% CO₂. Colonies were counted using a dissecting microscope after 10–14 days of culture.

Long-term competitive reconstitution assay

Test cells from *Plxdc2*^{+/+}, *Plxdc2*^{+/GFP}, and *Plxdc2*^{GFP/GFP} mice (CD45.2) were mixed with 2×10^5 CD45.1/CD45.2 adult BM MNCs and injected into adult recipient mice (CD45.1) irradiated at a dose of 9.5 Gy using a Cesium137 GammaCell40 Exactor Irradiator (MDS Nodria). PB cells were stained with

FITC-conjugated anti-CD45.1 antibodies, biotinylated anti-CD45.1 antibodies followed by APC-Cy7 streptavidin, PE-conjugated anti-Mac-1 and Gr-1 antibodies, APC-conjugated anti-CD4 and -CD8 antibodies, and PE-Cy7-conjugated anti-B220 antibodies. The test cell-derived chimerism was evaluated on a FACSCanto (BD Bioscience) system.

Blood count

PB was collected and analyzed on an automated blood cell counter, KX-21 (Sysmex), according to the manufacturer's instructions.

Human cord blood processing

All experiments using human CB cells were approved by the Ethics Committee at the Institute of Medical Science, the University of Tokyo (approval number: 27-34-1225). Human CB cells were obtained from the Japanese Red Cross Kanto-Koshinetsu Cord Blood Bank (Tokyo, Japan) following an institutional review board-approved protocol. Informed consent was obtained in accordance with the Declaration of Helsinki. Various CB samples were pooled, and an equal volume of PBS/2% FBS was added prior to layering on Lymphoprep™ (STEM CELL Technologies) in 50 mL conical tubes. Tubes were subjected to 30 min centrifugation at 800 $\times g$ followed by careful removal of mononuclear layer and washed with PBS/2% FBS. CD34⁺ cells were enriched by Direct CD34⁺ Progenitor Isolation Kit (Miltenyi Biotec) according to the manufacturer's protocol. CD34⁺ cells were stored in liquid nitrogen.

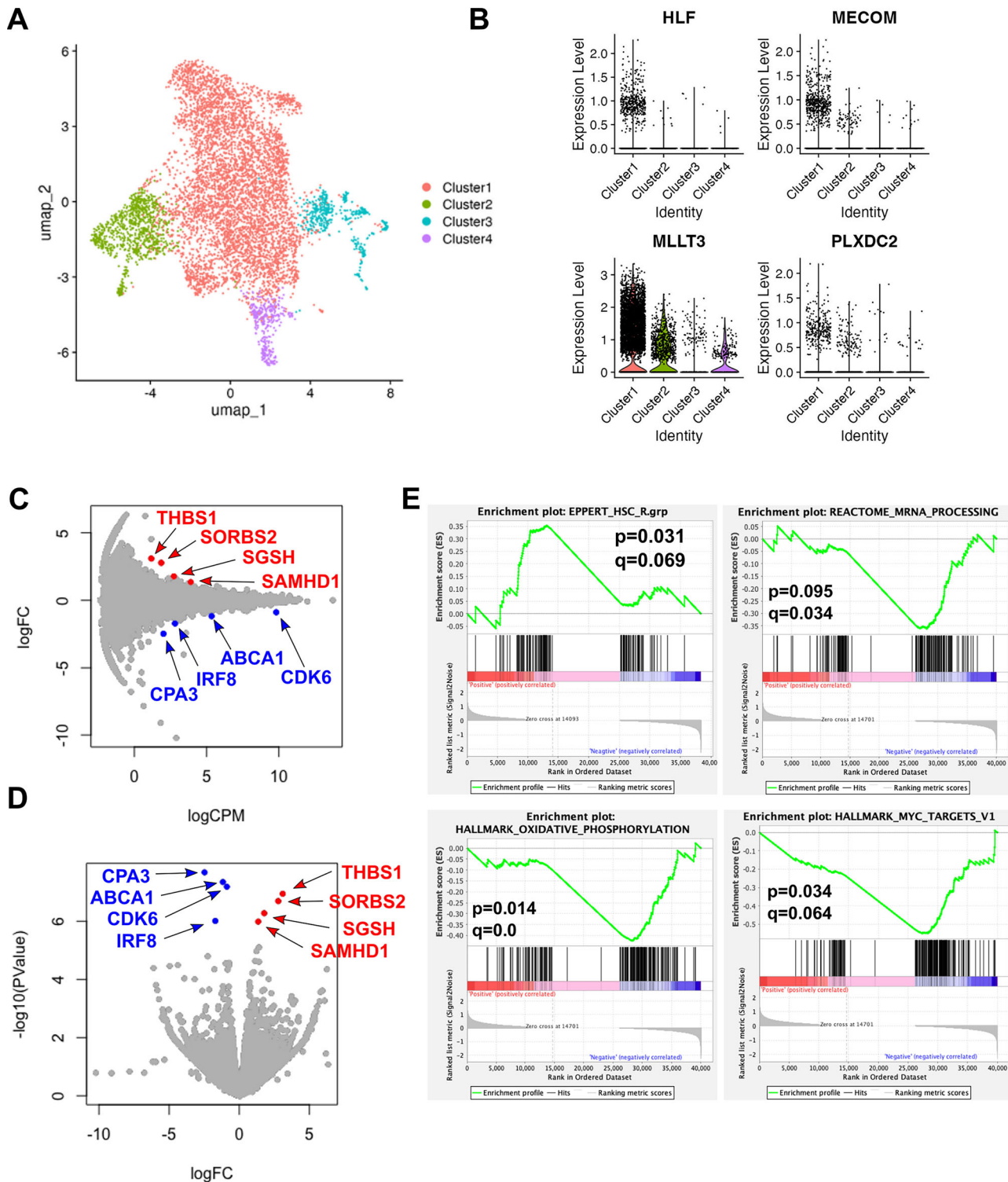


Fig. 5 | PLXDC2⁺ HSCs show more HSC signature. **A** Uniform manifold approximation and projection (UMAP) plot of single-cell RNA-seq data from two fresh cord blood cells from publicly available data (GSE153370)⁵⁰. **B** Violin plots displaying HLF, MECOM, MLLT3, and PLXDC2 expression in two fresh cord blood cells from publicly available data. The MA plot (C) and the volcano plot (D)

show eight genes differentially expressed (four genes upregulated in PLXDC2⁺ HSCs (red) and four genes upregulated in PLXDC2⁻ HSCs (blue), FDR < 0.05). **E** Gene set enrichment analysis (GSEA). NES normalized enrichment score. PLXDC2⁺ HSCs versus PLXDC2⁻ HSCs is represented.

Cell preparation for cell sorting

CD34⁺ cells were stained with CD45RA (FITC, clone HI100), CD90 (APC, clone 5E10), CD49f (PE-DazzleTM594, clone GoH3), CD34 (APC-Cy7, clone 581), CD38 (PE-Cy7, clone HIT2), Lineage marker cocktail (BV510, CD3/14/16/19/20//56, clone OKT3/M5E2/3G8/HIB19/2H7/HCD56)

(BioLegend) and PLXDC2 (PE/APC, rabbit monoclonal clone 4G3) (Kyokuto Pharmaceutical Industrial Co. Ltd. and Abwiz Bio Inc.) and incubated for 30 min at 4 °C. Cells were washed with PBS/2% FBS and stained with streptavidin conjugated BV605 (BioLegend) if a CD90 biotin-conjugated antibody was used. Cells were subsequently washed and

resuspended in PBS/2% FBS prior to sorting. Cells were sorted on FACS AriaII (Becton Dickinson) with a 100-micron nozzle operating mode and collected in 1.5 mL microtubes.

Xenotransplant assays

NOD.Cg-*Prkdc*^{scid}*Il2rg*^{tm1Wjl}/SzJ (NSG) (Jackson Laboratory) were purchased. Animal experiments were performed in accordance with institutional guidelines approved by the University of Tokyo. Various cell doses of PLXDC2⁺ or PLXDC2⁻ human HSCs were transplanted into 2.5 Gy irradiated NSG mice by tail vein injection.

Assessment of human cell engraftment

BM, thymus, PB, and spleen from NSG mice were analyzed for human cell engraftment with CD45 (BV421, clone). Cells were stained in PBS/2% FBS and analyzed by flow cytometry (FACSAriaII, Beckton Dickinson). Lineage committed cells in BM, PB, and spleen were analyzed with CD33 (PE, clone WM53), CD19(PE-Cy7, clone HIB19), and CD3 (FITC, clone OKT3). Thymocytes were analyzed with CD4 (FITC, clone OKT4) and CD8 (PE, clone SK1). Stem progenitor cells in BM were analyzed with CD34, CD38, CD90, CD45RA, CD49f, and PLXDC2. All antibodies used in this study were obtained from BioLegend unless otherwise indicated.

RNA-seq

We performed RNA-seq as described previously⁵¹ with minor modifications. In brief, using 100 sorted cells, the first strand of cDNA was synthesized by using PrimeScript RT reagent kit (TaKaRa Bio Inc.) and not-so-random primers. Following the synthesis of the first strand, the second strand was synthesized by using Klenow Fragment (30, _50, exo; New England Biolabs Inc.) and complement chains of not-so-random primers. Using purified double-strand cDNA, the library for RNA-Seq was prepared and amplified using Nextera XT DNA sample Prep kit (Illumina Inc.). These prepared libraries were sequenced on the Next-Seq system (Illumina Inc.), according to the manufacturer's instructions. In addition, each obtained read was mapped to the reference sequence "GRCh38" using CLC genomic workbench v11.0.0 (QIAGEN), and expression levels were normalized and subjected to statistical analyses based on EdgeR. Transcriptome data were subjected to GSEA using GSEA v3.0.0 software, available from the Broad Institute⁵². All Gene sets were obtained from the database of the Broad Institute unless otherwise stated. Principal component analysis, hierarchical clustering analysis, and visualization of gene expression or protein level were performed by Multi-expression Viewer.

Analysis of public single-cell RNA-seq data

Analysis was performed using Seurat v.4.0 (ref. 40) in R. HLF, MECOM, MLLT3, and PLXDC2 expression in fresh CB data was obtained from the Gene Expression Omnibus (GSE153370).

BM slice preparation, immunostaining, and optical clearing

Methods for 3D imaging of BM were adapted from previously published protocols⁵³. Femurs were isolated from *Plxdc2*^{GFP/+} mice, cleaned, and immersed in PBS/2% paraformaldehyde for 6 h at 4 °C, followed by a dehydration step in 30% sucrose for 72 h at 4 °C. Femurs were then embedded in cryopreserving medium (optimal cutting temperature (OCT)) and snap frozen in liquid nitrogen. Bone specimens were iteratively sectioned using a cryostat until the BM cavity was fully exposed along the longitudinal axis. The OCT block containing the bone was then reversed, and the procedure was repeated on the opposite face until a thick bone slice with bilaterally and evenly exposed BM content was obtained. Once the BM slices were generated, the remaining OCT medium was removed by incubation and washing of the bone slices in PBS three times for 5 min. For immunostaining, slices were incubated in blocking solution (0.2% Triton X-100, 5% skim milk, 1% bovine serum albumin (BSA), 10% donkey serum in PBS) overnight at 4 °C.

Primary antibody incubations were performed in blocking solution for 3 days at 4 °C, followed by overnight washing in PBS. Secondary antibody stainings were performed for another 3 days at 4 °C in blocking solution but in the absence of BSA to avoid cross-absorption. Immunostained thick femoral slices were successively washed in PBS overnight and incubated in RapiClear 1.52 for a minimum of 6 h, which typically increased imaging depth to 150 µm from the tissue surface without significant loss of signal intensity. The clearing protocol employed is fast, compatible with all fluorescent probes and proteins tested, and preserves the integrity of subcellular structures.

Preparation of PBMC

Human PBMCs were isolated from the peripheral venous blood of healthy volunteers, as described previously⁵⁴. Briefly, whole blood (20 mL) was mixed with 7 mL of a 6% dextran solution and 15 mL of HBSS(−) (Gibco) and allowed to stand for 30 min at 25 °C until stratification occurred. The upper leukocyte-rich plasma layer was transferred to a new tube containing endotoxin-free Ficoll-Paque PLUS gradient (GE Healthcare Japan, Tokyo, Japan) and was centrifuged (500 × g, 30 min, 25 °C). The cell layer was harvested, and subsequently, the cells were resuspended at 100 million PBMC per mL in PBS. Monocyte Attachment Medium (Promocell, Heidelberg, Germany) HBSS. The protocol was approved by the Ethical Review Committee at the Teikyo University School of Medicine (no. 15-192-2). All participants gave written informed consent prior to their inclusion in the study. All ethical regulations relevant to human research participants were followed.

Preparation of PBMC Lysate

Human PBMCs (up to 1 × 10⁷ cells) were lysed using the Mem-PER Plus Membrane Protein Extraction Kit (Thermo Fisher Scientific, Waltham, USA) in the presence of a protease inhibitor cocktail (Cell Signaling Technology, Danvers, MA), following the manufacturer's instructions. Briefly, the cells were harvested by centrifugation at 180 × g for 5 min and washed twice with 1 mL of Cell Wash Solution (Thermo Fisher Scientific). The washed cell pellets were resuspended in 300 µL of Permeabilization Buffer (Thermo Fisher Scientific) containing a protease inhibitor cocktail and incubated for 15 min at 4 °C. The lysate was then centrifuged at 16,000 × g for 15 min at 4 °C, and the supernatant containing the cytosolic fraction was carefully transferred to a new tube. The pellet was resuspended in 100 µL of Solubilizing Buffer (Thermo Fisher Scientific) containing a protease inhibitor cocktail and incubated at 4 °C for 30 min with constant mixing. This suspension was subsequently centrifuged at 16,000 × g for 15 min at 4 °C, and the resulting supernatant, containing the membrane fraction, was carefully transferred to a new tube. Protein concentrations in both fractions were determined using the BCA assay.

SDS-PAGE

The cytosolic and membrane fractions (10 µg/lane) of PBMCs or human platelet lysate (50 or 250 µg/lane) (UltraGRO, AventaCell biomedical, New Taipei, Taiwan) were analyzed by SDS-PAGE using a 7.5% Super-Sep gel (Fujifilm Wako Chemicals, Tokyo, Japan). A pre-stained protein marker, Precision Plus Protein Dual Color Standards (Bio-Rad, CA, USA), was used as a reference. Electrophoresis was conducted at a constant current of 25 mA for 50 min. Following electrophoresis, gels were stained with Coomassie Brilliant Blue.

Western blotting

Proteins were transferred from the gel to a PVDF membrane using an electrical blotting system, following the Bio-Rad manual. After transfer, the PVDF membranes were blocked with a PVDF blocking solution (TOYOBIO, Tokyo, Japan) for 1 h. For the detection of

PLXDC2 in PBMC, the membranes were incubated at room temperature (RT) for 24–48 h with primary antibodies: either a biotinylated rabbit monoclonal antibody (4G3, Abwiz Bio, 1:1000) or a rabbit polyclonal antibody (ab67226, Abcam, 1:2000), diluted in Can Get Signal 1 solution (TOYOB). To detect the primary antibody, membranes were treated at RT for 1 h with streptavidin-poly-HRP80 (Stereospecific Detection Technologies GmbH, Baesweiler, Germany) for 4G3 or with a combination of biotinylated anti-rabbit IgG (H+L) antibody (#14708, CST) and streptavidin-poly-HRP80 for rabbit polyclonal antibody. Antibody binding was visualized using EzWest Blue (ATTO, Tokyo, Japan).

For the detection of PLXDC2 in human platelets, membranes were incubated at RT for 24 h with primary antibodies—either a clone 4G3 (1:2000) or a rabbit polyclonal antibody (12285-1-AP, Proteintech, 1:2000)—diluted in Can Get Signal 1 solution (TOYOB). To detect the bound primary antibodies, membranes were then incubated at RT for 1 h with an HRP-conjugated anti-rabbit IgG secondary antibody (#7074, CST, 1:5000), diluted in TBS-T. Antibody binding was visualized using SuperSignal Western Blot Enhancer (Thermo Fisher Scientific). Chemiluminescent signals were captured using the ImageQuant LAS 500 system (Cytiva, Japan).

Statistics and reproducibility

Data for each experiment were collected from a minimum of three biological replicates. Quantitative data were analyzed using GraphPad Prism (10.1.0) employing unpaired Student's *t*-test or one- or two-way ANOVA without correction for multiple comparison (Fisher LSD test). All data are presented as mean \pm SEM. Significance levels were set at ${}^*p < 0.05$, ${}^{**}p < 0.01$, and ${}^{***}p < 0.001$. For statistical analysis, GraphPad Prism was used.

Reporting summary

Further information on research design is available in the Nature Portfolio Reporting Summary linked to this article.

Data availability

The RNA-sequencing data have been deposited in the NCBI Gene Expression Omnibus under the accession code GSE303568. Source data are provided with this paper.

Materials availability

Plxdc2-GFP knock-in mice are available from Columbia University with a material transfer agreement (MTA). The human PLXDC2 monoclonal antibody generated in this study is also available from Kyokuto Pharmaceutical Industrial Co., Ltd and Abwiz Bio Inc.

Received: 11 September 2024; Accepted: 12 November 2025;

Published online: 10 December 2025

References

- Spangrude, G. J., Heimfeld, S. & Weissman, I. L. Purification and Characterization Of Mouse Hematopoietic Stem Cells. *Science* **241**, 58–62 (1988).
- Osawa, M., Hanada, K. I., Hamada, H. & Nakauchi, H. Long-term lymphohematopoietic reconstitution by a single CD34-low/negative hematopoietic stem cell. *Science* **273**, 242–245 (1996).
- Spangrude, G. J. Long-term repopulation of irradiated mice with limiting numbers of purified hematopoietic stem cells: in vivo expansion of stem cell phenotype but not function. *Blood* **85**, 11 (1995).
- Kiel, M. J. et al. SLAM family receptors distinguish hematopoietic stem and progenitor cells and reveal endothelial niches for stem cells. *Cell* **121**, 1109–1121 (2005).
- Mayani, H. & Dragowska, W. Characterization of functionally distinct subpopulations of CD34+ cord blood cells in serum-free long-term cultures supplemented with hematopoietic cytokines. *Blood* **82**, 2664–2672 (1993).
- Baum, C. M. & Peault, B. Isolation of a candidate human hematopoietic stem-cell population. *Proc. Natl. Acad. Sci. USA* **89**, 2804–2808 (1992).
- Craig, W., Kay, R., Cutler, R. L. & Lansdorp, P. M. Expression of Thy-1 on human hematopoietic progenitor cells. *J. Exp. Med.* **177**, 1331–1342 (1993).
- Majeti, R., Park, C. Y. & Weissman, I. L. Identification of a hierarchy of multipotent hematopoietic progenitors in human cord blood. *Cell Stem Cell* **1**, 635–645 (2007).
- Hao, Q., Shah, A., Thiemann, F., Smogorzewska, E. & Crooks, G. A functional comparison of CD34 + CD38- cells in cord blood and bone marrow. *Blood* **86**, 3745–3753 (1995).
- Bhatia, M., Wang, J. C. Y., Kapp, U., Bonnet, D. & Dick, J. E. Purification of primitive human hematopoietic cells capable of repopulating immune-deficient mice. *Proc. Natl. Acad. Sci. USA* **94**, 5320–5325 (1997).
- Notta, F. et al. Isolation of single human hematopoietic stem cells capable of long-term multilineage engraftment. *Science* **333**, 218–221 (2011).
- Visser, J. W., Bauman, J. G., Mulder, A. H., Eliason, J. F. & de Leeuw, A. M. Isolation of murine pluripotent hemopoietic stem cells. *J. Exp. Med.* **159**, 1576–1590 (1984).
- Christensen, J. L. & Weissman, I. L. Flk-2 is a marker in hematopoietic stem cell differentiation: a simple method to isolate long-term stem cells. *Proc. Natl. Acad. Sci. USA* **98**, 14541–14546 (2001).
- Chen, C. Z. et al. Identification of endoglin as a functional marker that defines long-term repopulating hematopoietic stem cells. *Proc. Natl. Acad. Sci. USA* **99**, 15468–15473 (2002).
- Balazs, A. B., Fabian, A. J., Esmon, C. T. & Mulligan, R. C. Endothelial protein C receptor (CD201) explicitly identifies hematopoietic stem cells in murine bone marrow. *Blood* **107**, 2317–2321 (2006).
- Yokota, T. et al. The endothelial antigen ESAM marks primitive hematopoietic progenitors throughout life in mice. *Blood* **113**, 2914–2923 (2009).
- Ooi, A. G. L. et al. The adhesion molecule Esam1 is a novel hematopoietic stem cell marker. *Stem Cells* **27**, 653–661 (2009).
- Morita, Y., Ema, H. & Nakauchi, H. Heterogeneity and hierarchy within the most primitive hematopoietic stem cell compartment. *J. Exp. Med.* **207**, 1173–1182 (2010).
- Yamamoto, R. et al. Clonal analysis unveils self-renewing lineage-restricted progenitors generated directly from hematopoietic stem cells. *Cell* **154**, 1112–1126 (2013).
- Gazit, R. et al. Fgd5 identifies hematopoietic stem cells in the murine bone marrow. *J. Exp. Med.* **211**, 1315–1331 (2014).
- Chen, J. Y. et al. Hoxb5 marks long-term haematopoietic stem cells and reveals a homogenous perivascular niche. *Nature* **530**, 223–227 (2016).
- Acar, M. et al. Deep imaging of bone marrow shows non-dividing stem cells are mainly perisinusoidal. *Nature* **526**, 126–130 (2015).
- Chao, M. P., Seita, J. & Weissman, I. L. Establishment of a normal hematopoietic and leukemia stem cell hierarchy. *Cold Spring Harb. Symp. Quant. Biol.* **73**, 439–449 (2008).
- Kubota, Y., Osawa, M., Jakt, L. M., Yoshikawa, K. & Nishikawa, S.-I. Necdin restricts proliferation of hematopoietic stem cells during hematopoietic regeneration. *Blood* **114**, 4383–4392 (2009).
- Miller, S. F. C. et al. Expression of Plxdc2/TEM7R in the developing nervous system of the mouse. *Gene Expr. Patterns* **7**, 635–644 (2007).
- Miller-Delaney, S. F. C., Lieberam, I., Murphy, P. & Mitchell, K. J. Plxdc2 is a mitogen for neural progenitors. *PLoS ONE* **6**, e14565 (2011).

27. Cheng, G. et al. Identification of PLXDC1 and PLXDC2 as the transmembrane receptors for the multifunctional factor PEDF. *eLife* **3**, e05401 (2014).

28. Bianchi, E. et al. Control of oviductal fluid flow by the G-protein coupled receptor Adgrd1 is essential for murine embryo transit. *Nat. Commun.* **12**, 1251 (2021).

29. Tubau-Juni, N. et al. Identification of new regulatory genes through expression pattern analysis of a global RNA-seq dataset from a *Helicobacter pylori* co-culture system. *Sci. Rep.* **10**, 11506 (2020).

30. Shimizu, H. et al. Improving the quality of a recombinant rabbit monoclonal antibody against PLXDC2 by optimizing transient expression conditions and purification method. *Protein Expr. Purif.* **146**, 27–33 (2018).

31. Laurenti, E. et al. CDK6 levels regulate quiescence exit in human hematopoietic stem cells. *Cell Stem Cell* **16**, 302–313 (2015).

32. Cabezas-Wallscheid, N. et al. Vitamin A-retinoic acid signaling regulates hematopoietic stem cell dormancy. *Cell* **169**, 807–823.e19 (2017).

33. Fukushima, T. et al. Discrimination of dormant and active hematopoietic stem cells by G0 marker reveals dormancy regulation by cytoplasmic calcium. *Cell Rep.* **29**, 4144–4158 (2019).

34. Kurotaki, D. et al. Essential role of the IRF8-KLF4 transcription factor cascade in murine monocyte differentiation. *Blood* **121**, 1839–1849 (2013).

35. Kurotaki, D. et al. Transcription factor IRF8 governs enhancer landscape dynamics in mononuclear phagocyte progenitors. *Cell Rep.* **22**, 2628–2641 (2018).

36. Georgantas, R. W. et al. Microarray and serial analysis of gene expression analyses identify known and novel transcripts overexpressed in hematopoietic stem cells. *Cancer Res.* **64**, 4434–4441 (2004).

37. Fares, I. et al. Pyrimidoindole derivatives are agonists of human hematopoietic stem cell self-renewal. *Science* **345**, 1509–1512 (2014).

38. Fares, I. et al. EPCR expression marks UM171-expanded CD34+ cord blood stem cells. *Blood* **129**, 3344–3351 (2017).

39. Ishibashi, T. et al. ESAM is a novel human hematopoietic stem cell marker associated with a subset of human leukemias. *Exp. Hematol.* **44**, 269–281.e1 (2016).

40. Murphy-Ullrich, J. E. & Pocztak, M. Activation of latent TGF- β by thrombospondin-1: mechanisms and physiology. *Cytokine Growth Factor Rev.* **11**, 59–69 (2000).

41. Yamazaki, S. et al. Nonmyelinating Schwann cells maintain hematopoietic stem cell hibernation in the bone marrow niche. *Cell* **147**, 1146–1158 (2011).

42. Wang, B., Golemis, E. A. & Kruh, G. D. ArgBP2, a multiple Src homology 3 domain-containing, Arg/Abl-interacting protein, is phosphorylated in v-Abl-transformed cells and localized in stress fibers and cardiocyte Z-disks. *J. Biol. Chem.* **272**, 17542–17550 (1997).

43. Zhao, L. et al. The RNA binding protein SORBS2 suppresses metastatic colonization of ovarian cancer by stabilizing tumor-suppressive immunomodulatory transcripts. *Genome Biol.* **19**, 35 (2018).

44. Lu, J. et al. Fak depletion in both hematopoietic and nonhematopoietic niche cells leads to hematopoietic stem cell expansion. *Exp. Hematol.* **40**, 307–317.e3 (2012).

45. Batista, S. et al. Haematopoietic focal adhesion kinase deficiency alters haematopoietic homeostasis to drive tumour metastasis. *Nat. Commun.* **5**, 5054 (2014).

46. Loeffler, D. et al. Asymmetric lysosome inheritance predicts activation of haematopoietic stem cells. *Nature* **573**, 426–429 (2019).

47. Laguette, N. et al. SAMHD1 is the dendritic- and myeloid-cell-specific HIV-1 restriction factor counteracted by Vpx. *Nature* **474**, 654–657 (2011).

48. Hrecka, K. et al. Vpx relieves inhibition of HIV-1 infection of macrophages mediated by the SAMHD1 protein. *Nature* **474**, 658–661 (2011).

49. Wu, X. et al. Intrinsic Immunity Shapes Viral Resistance of Stem Cells. *Cell* **172**, 423–438.e25 (2018).

50. Lehnertz, B. et al. HLF expression defines the human hematopoietic stem cell state. *Blood* **138**, 2642–2654 (2021).

51. Hayashi, T. et al. Single-cell full-length total RNA sequencing uncovers dynamics of recursive splicing and enhancer RNAs. *Nat. Commun.* **9**, 619 (2018).

52. Subramanian, A. et al. Gene set enrichment analysis: a knowledge-based approach for interpreting genome-wide expression profiles. *Proc. Natl. Acad. Sci. USA* **102**, 15545–15550 (2005).

53. Gomariz, A. et al. Quantitative spatial analysis of haematopoiesis-regulating stromal cells in the bone marrow microenvironment by 3D microscopy. *Nat. Commun.* **9**, 2532 (2018).

54. Sato, Y., Unno, Y., Miyazaki, C., Ubagai, T. & Ono, Y. Multidrug-resistant *Acinetobacter baumannii* resists reactive oxygen species and survives in macrophages. *Sci. Rep.* **9**, 17462 (2019).

Acknowledgements

The authors thank Shiori Shikata and Akiho Tsuchiya for expert technical assistance. The authors thank the IMSUT FACS Core Laboratory and the IMSUT Animal Research Center. This work was supported by a Grant-in-Aid for Challenging Exploratory Research (17K19645, Y.T.), KAKENHI grant number (20K07639, Y.K.), a grant from The SENSIN Medical Research Foundation (Y.T.), a grant from Leukemia Research Fund (S.G.), Tokyo Metropolitan Small and Medium Enterprise Support Center (T.A. and Y.T.), and MRC-AMED joint award (MR/V005502/1) (D.G.K. and Y.T.). The authors finally thank Shin-ichi Nishikawa for supervision of starting this study.

Author contributions

Conceptualization and methodology: Y.T., T.A. and Y.K.; investigation: Y.T., Y.K., T.F., Y.A., T.K., T.Y., J.L.B., R.K., Y.S., Y.O., H.M. and J.W.B.; visualization: C.S., T.S., M.N., Y.K., T.M. and T.A.; writing—original draft: Y.T.; writing—review and editing: Y.T., Y.K., D.G.K., S.Y. and T.S.; funding acquisition: Y.T., T.A., D.G.K. and Y.K.; resources: Y.T., Y.K., S.G., I.L., C.S., T.S., M.N., Y.K., T.M., C.J.O., T.A., H.N. and T.M.J.; supervision: S.K., T.A., and T.K.

Competing interests

The authors declare no competing interests.

Additional information

Supplementary information The online version contains supplementary material available at <https://doi.org/10.1038/s42003-025-09242-x>.

Correspondence and requests for materials should be addressed to Yosuke Tanaka or Yasushi Kubota.

Peer review information *Communications Biology* thanks the anonymous reviewers for their contribution to the peer review of this work. Primary Handling Editor: Dario Ummarino. A peer review file is available.

Reprints and permissions information is available at <http://www.nature.com/reprints>

Publisher's note Springer Nature remains neutral with regard to jurisdictional claims in published maps and institutional affiliations.

Open Access This article is licensed under a Creative Commons Attribution-NonCommercial-NoDerivatives 4.0 International License, which permits any non-commercial use, sharing, distribution and reproduction in any medium or format, as long as you give appropriate credit to the original author(s) and the source, provide a link to the Creative Commons licence, and indicate if you modified the licensed material. You do not have permission under this licence to share adapted material derived from this article or parts of it. The images or other third party material in this article are included in the article's Creative Commons licence, unless indicated otherwise in a credit line to the material. If material is not included in the article's Creative Commons licence and your intended use is not permitted by statutory regulation or exceeds the permitted use, you will need to obtain permission directly from the copyright holder. To view a copy of this licence, visit <http://creativecommons.org/licenses/by-nc-nd/4.0/>.

© The Author(s) 2025

¹Division of Cell Regulation, Center for Experimental Medicine and Systems Biology, The Institute of Medical Science, The University of Tokyo, Tokyo, Japan.

²Laboratory of Stem Cell Regulation, International Research Center for Medical Sciences, Kumamoto University, Kumamoto, Japan. ³Division of Hematology, Respiratory Medicine and Oncology, Department of Internal Medicine, Faculty of Medicine, Saga University, Saga, Japan. ⁴Department of Clinical Laboratory Medicine, Saga-ken Medical Centre KOSEIKAN, Saga, Japan. ⁵Department of Hematology, Faculty of Medicine, University of Tsukuba, Tsukuba, Japan. ⁶Centre for Gene Therapy and Regenerative Medicine and Centre for Developmental Neurobiology, King's College London, London, UK. ⁷Department of Biology, York Biomedical Research Institute, University of York, York, UK. ⁸Kyokuto Pharmaceutical Industrial Co., Ltd, Tokyo, Japan. ⁹Abwiz Bio, Inc., San Diego, CA, USA. ¹⁰Department of Anatomy, Faculty of Life Sciences, Kumamoto University, Kumamoto, Japan. ¹¹Department of Microbiology and Immunology, Teikyo University School of Medicine, Tokyo, Japan. ¹²Faculty of Health and Medical Science, Teikyo Heisei University, Tokyo, Japan. ¹³Laboratory of Multi-dimensional imaging, International Research Center for Medical Sciences, Kumamoto University, Kumamoto, Japan. ¹⁴Howard Hughes Medical Institute, Zuckerman Institute, Depts. of Neuroscience, and Biochemistry and Molecular Biophysics, Columbia University, New York, NY, USA. ¹⁵Division of Molecular Oncology, Department of Computational Biology and Medical Sciences, Graduate School of Frontier Sciences, The University of Tokyo, Tokyo, Japan. ¹⁶Division of Cellular Therapy, The Institute of Medical Science, The University of Tokyo, Tokyo, Japan. ¹⁷These authors contributed equally: Yosuke Tanaka, Yasushi Kubota. ¹⁸Deceased: Yasunori Kurosawa. ¹⁹Deceased: Thomas M. Jessell.

✉ e-mail: yosuketa@g.ecc.u-tokyo.ac.jp; kubota-yasushi@koseikan.jp